J|A|C|S
ARTICLES

Published on Web 05/08/2008

Photoluminescence of Perovskite Nanosheets Prepared by Exfoliation of Layered Oxides, $K_2Ln_2Ti_3O_{10}$, $KLnNb_2O_7$, and $RbLnTa_2O_7$ (Ln: Lanthanide Ion)

Shintaro Ida,*,† Chikako Ogata,† Miharu Eguchi,‡ W. Justin Youngblood,‡ Thomas E. Mallouk,‡ and Yasumichi Matsumoto†

Graduate School of Science and Technology, Kumamoto University, 2-39-1 Kurokami, Kumamoto 860-8555, Japan and Department of Chemistry, The Pennsylvania State University, University Park, Pennsylvania 16802

Received December 30, 2007; E-mail: s_ida@chem.chem.kumamoto-u.ac.jp

Abstract: Luminescent perovskite nanosheets were prepared by exfoliation of single- or double- layered perovskite oxides, $K_2Ln_2Ti_3O_{10}$, $KLnNb_2O_7$, and $RbLnTa_2O_7$ (Ln: lanthanide ion). The thickness of the individual nanosheets corresponded to those of the perovskite block in the parent layered compounds. Intense red and green emissions were observed in aqueous solutions with $Gd_{1.4}Eu_{0.6}Ti_3O_{10}$- and $La_{0.7}Tb_{0.3}Ta_2O_7$-nanosheets, respectively, under UV illumination with energies greater than the corresponding host oxide band gap. The coincidence of the excitation spectrum and the band gap absorbance indicates that the visible emission results from energy transfer within the nanosheet. The red emission intensity of the $Gd_{1.4}Eu_{0.6}Ti_3O_{10}$-nanosheets was much stronger than that of the $La_{0.90}Eu_{0.05}Nb_2O_7$-nanosheets reported previously. The strong emission intensity is a result of a two-step energy transfer cascade within the nanosheet from the Ti−O network to Gd^{3+} and then to Eu^{3+}. The emission intensities of the $Gd_{1.4}Eu_{0.6}Ti_3O_{10}$- and $La_{0.7}Tb_{0.3}Ta_2O_7$-nanosheets can be modulated by applying a magnetic field (1.3−1.4 T), which brings about a change in orientation of the nanosheets in solution. The emission intensities increased when the excitation light and the magnetic field directions were perpendicular to each other, and they decreased when the excitation and magnetic field were collinear and mutually perpendicular to the direction of detection of the emitted light.

Introduction

Luminescent nanoparticles have attracted much attention as promising component materials for optical and electro-optical devices,[1–3] which require well-organized nanostructures. Luminescent nanoparticles have been developed in a number of shapes, including spheres,[4–6] nanowires,[7,8] nanorods,[9] and nanotubes.[10] Recently, two-dimensional nanosheets have been prepared by exfoliation of layered oxides.[11–20] A luminescent nanosheet has a geometric advantage over other types of particles, because highly oriented films can be easily grown be layer-by-layer[21–23] and Langmuir−Blodgett (LB)[24–26] tech-

† Kumamoto University.
‡ The Pennsylvania State University.
(1) Duan, X.; Huang, Y.; Cui, Y.; Wang, J.; Lieber, C. M. *Nature* **2001**, *409*, 66–69.
(2) Coe, S.; Woo, W.-K.; Bawendi, M.; Bulovic, V. *Nature* **2002**, *420*, 800–803.
(3) Colvin, V. L.; Schlamp, M. C.; Alivisatos, A. P. *Nature* **1994**, *370*, 354–357.
(4) Bruchez, M., Jr.; Moronne, M.; Gin, P.; Weiss, W.; Alivisatos, A. P. *Science* **1998**, *281*, 2013–2016.
(5) Tang, Z.; Kotov, N. A.; Giersig, M. *Science* **2002**, *297*, 237–240.
(6) Milliron, D. J.; Hughes, S. M.; Cui, Y.; Manna, L.; Li, J.; Wang, L.-W.; Alivisatos, A. P. *Nature* **2004**, *430*, 190–195.
(7) Duan, X.; Huang, Y.; Agarwal, R.; Lieber, C. M. *Nature* **2003**, *421*, 241–245.
(8) Nakayama, Y.; Pauzauskie, P. J.; Radenovic, A.; Onorato, R. M.; Saykally, R. J.; Liphardt, J.; Yang, P. *Nature* **2007**, *447*, 1098–1103.
(9) Hu, J.; Li, L.-S.; Wang, L.-W.; Manna, L.; Wang, L.; Alivisatos, A. P. *Science* **2001**, *292*, 2060–2063.
(10) O'Connell, M. J.; Bachilo, S. M.; Huffman, C. B.; Moore, V. C.; Strano, M. S.; Haroz, E. H.; Rialon, K. L.; Boul, P. J.; Noon, W. H.; Kittrell, C.; Ma, J.; Hauge, R. H.; Weisman, R. B.; Smalley, R. E. *Science* **2002**, *297*, 593–596.
(11) Sasaki, T.; Watanabe, M.; Hashizume, H.; Yamada, H.; Nakazawa, H. *J. Am. Chem. Soc.* **1996**, *118*, 8329–8335.
(12) Schaak, R. E.; Mallouk, T. E. *Chem. Mater.* **2000**, *12*, 2513–2516.
(13) Kudo, A.; Tanaka, A.; Domen, K.; Maruya, K.; Aika, K.; Onishi, T. *J. Catal.* **1988**, *111*, 67–76.
(14) Sasaki, T.; Watanabe, M. *J. Am. Chem. Soc.* **1998**, *120*, 4682–4689.
(15) Han, Y.-S.; Park, I.; Choy, J.-H. *J. Mater. Chem.* **2001**, *11*, 1277–1282.
(16) Schaak, R. E.; Mallouk, T. E. *Chem. Mater.* **2000**, *12*, 3427–3434.
(17) Ma, R.; Liu, Z.; Takada, K.; Iyi, N.; Bando, Y.; Sasaki, T. *J. Am. Chem. Soc.* **2007**, *129*, 5257–5263.
(18) Ida, S.; Ogata, C.; Unal, U.; Izawa, K.; Inoue, T.; Altuntasoglu, O.; Matsumoto, Y. *J. Am. Chem. Soc.* **2007**, *129*, 8956–8957.
(19) Ozawa, T. C.; Fukuda, K.; Akatsuka, K.; Ebina, Y.; Sasaki, T. *Chem. Mater.* **2007**, *19*, 6575–6580.
(20) Ozawa, T. C.; Fukuda, K.; Akatsuka, K.; Ebina, Y.; Sasaki, T.; Kurashima, K.; Kosuda, K. *J. Phys. Chem. C* **2008**, *112*, 1312–1315.
(21) Hata, H.; Kubo, S.; Kobayashi, Y.; Mallouk, T. E. *J. Am. Chem. Soc.* **2007**, *129*, 3064–3065.
(22) Zhou, Y.; Ma, R.; Ebina, Y.; Takada, K.; Sasaki, T. *Chem. Mater.* **2006**, *18*, 1235–1239.
(23) Sasaki, T.; Ebina, Y.; Watanabe, M.; Decher, G. *Chem. Commun.* **2000**, *21*, 2163–2164.
(24) Muramatsu, M.; Akatsuka, K.; Ebina, Y.; Wang, K.; Sasaki, T.; Ishida, T.; Miyake, K.; Haga, M. *Langmuir* **2005**, *21*, 6590–6595.
(25) Akatsuka, K.; Ebina, Y.; Muramatsu, M.; Sato, T.; Hester, H.; Kumaresan, D.; Schmehl, R. H.; Sasaki, T.; Haga, M. *Langmuir* **2007**, *23*, 6730–6736.

10.1021/ja7114772 CCC: $40.75 © **2008 American Chemical Society**

niques. As oxides, they are chemically robust and are likely to be less susceptible to the photobleaching problems of organic dyes and polymers. In addition, because most of the atoms that constitute the nanosheets are in direct contact with adsorbed chemical species, such as H^+ and OH^-, their luminescence properties are affected by adsorption.[18] Thus, luminescent nanosheets have the potential to be useful not only as materials for next-generation optical and electro-optical devices but also as the luminescent probes for chemical and bioanalytical sensors. We have reported the blue emitting nanosheets prepared by exfoliation of $Bi_2SrTa_2O_9$.[18] Recently, Ozawa et al. reported the red emitting nanosheets prepared by exfoliation of $KLa_{0.90}Eu_{0.05}Nb_2O_7$ and $Li_2Eu_{0.56}Ta_2O_7$.[19,20] If intense red-, green-, and blue-emitting nanosheets can be developed, then luminescent devices with full chromaticity might be fabricated by building up layers of nanosheets or by combining them in fluid suspensions.

Dynamic control of the orientation of luminescent nanosheets in solution can open up new possibilities for applications. It is known that the transparency and absorption of light of colloidal suspensions of nanosheets (also called nanosheet solutions) can be changed by the sol−gel transition, as in the case of liquid crystals. For example, Nakato et al. have studied the liquid crystalline ordering of Nb_6O_{17}-nanosheets and pH-induced switching to oriented gels.[27–30] These phenomena are a consequence of the two-dimensional character of the nanosheets. However, it is difficult to achieve rapid reorientation of the nanosheets and optical switching in this way, because the response of the sol−gel transition is slow.

In this paper, we demonstrate that the $Gd_{(2-x)}Eu_xTi_3O_{10}$- and $La_{(1-x)}Tb_xTa_2O_7$-nanosheets give intense red and green emissions, respectively, under UV illumination at room temperature. In addition, we find that the emission intensity of the suspended nanosheets can be modulated dynamically by changing their orientation in a relatively modest (∼1 T) magnetic field.

Experimental Section

Materials. Three families of layered perovskites, $K_2Ln_2Ti_3O_{10}$ (Ln: La, Pr, Sm, Nd, Eu, Gd, Tb, Dy), $KLnNb_2O_7$ (Ln: La), and $RbLnTa_2O_7$ (Ln: La, Gd), were prepared as starting materials (see Supporting Information S1). Red and green emissions can be obtained by substituting the Ln^{3+} sites (A sites) in these layered oxides with Eu^{3+} or Tb^{3+}. Specific synthetic procedures have been described in detail elsewhere.[31–37] $K_2Ln_{1.9}Eu_{0.1}Ti_3O_{10}$, $K_2Ln_{1.9}Tb_{0.1}Ti_3O_{10}$, and $K_2Gd_{2-x}Eu_xTi_3O_{10}$ (x = 0, 0.02, 0.04, 0.1, 0.2, 0.6, 1, and 2) were prepared by reacting stoichiometric amounts of intimately mixed K_2CO_3, La_2O_3, Pr_2O_3, Nd_2O_3, Sm_2O_3, Eu_2O_3, Gd_2O_3, Tb_4O_7, Dy_2O_3, and TiO_2 at 1050 °C for 5 h. $KLa_{0.95}Eu_{0.05}Nb_2O_7$ and $KLa_{0.95}Tb_{0.05}Nb_2O_7$ were prepared by reacting stoichiometric amounts of intimately mixed K_2CO_3, La_2O_3, Eu_2O_3, Tb_4O_7, and Nb_2O_5 at 900 °C for 4 h and subsequently at 1100 °C for 40 h. $RbLn_{0.95}Eu_{0.05}Ta_2O_7$, $RbLn_{0.95}Tb_{0.05}Ta_2O_7$, and $RbLa_{1-x}Tb_xTa_2O_7$ (x = 0.05, 0.1, 0.3, 0.5, and 1) were prepared by reacting stoichiometric amounts of intimately mixed Rb_2CO_3, La_2O_3, Gd_2O_3, Eu_2O_3, Tb_2O_3, and Ta_2O_5 at 1000−1100 °C for 12−40 h in the air. In the cases of $K_2Ln_2Ti_3O_{10}$ and $RbLnTa_2O_7$, a 40% excess of the alkali source was used to compensate for the loss due to volatilization. In the cases of $RbLa_{1-x}Tb_xTa_2O_7$, the sintering processes were performed in 100% Ar gas to avoid oxidation of Tb^{3+}.

Protonation and Exfoliation. Protonation was carried out by stirring 1.0 g of the as-prepared layered perovskite powder in 100 mL of 1 M aqueous HCl solution for 5 days at room temperature. In all cases, the acid was replaced three times to ensure complete exchange. After the reaction, the solid products were centrifuged and washed with distilled water. Exfoliation was typically achieved by reacting 0.5 g of the protonated solid products with 100 mL of a 0.1 M ethylamine solution at room temperature for 5 days. The suspensions were then centrifuged at 3000 rpm for 30 min, and the supernatants were used as the nanosheet solutions.

Characterization and Equipment. The crystal structure was analyzed using X-ray powder diffraction patterns (using Cu Kα radiation, Rigaku RINT-2500VHF). The compositions of the nanosheets were determined by means of an inductively coupled plasma (ICP) spectrophotometer (Seiko Instruments, SPS7800). The concentration of the nanosheets in the solution was adjusted to 2×10^{-5} M (formula unit) on the basis of the results of ICP analysis (preparation of the samples for ICP measurement: see Supporting Information S2). UV−vis absorption spectra were obtained using a Jasco V-550 spectrometer. Excitation and emission spectra were obtained using a Jasco FP-6500 spectrofluorometer with a 150-W Xe lamp at room temperature. The excitation and emission spectra were corrected for the spectral distribution of the Xe lamp intensity by the Rhodamine by the RB (5.5g/L, ethylene glycol solution) and a JASCO ESC-333 reference light source. The emission decay curves of nanosheet solutions were plotted on the basis of the time-resolved emission spectra, which were obtained by using a Perkin-Elmer LS 55 fluorescence spectrometer. The relative photoluminescence efficiencies of the emission of the nanosheet solution were estimated by comparison with solutions of quinine in aqueous 0.5 M H_2SO_4 (quantum yield: 54.6%).[38] The square quartz cell was used for the above photoluminescence measurement. The absolute quantum yields of solid samples were determined by standard procedures using a spectrofluorometer (JASCO FP-6500) equipped with an integrating sphere (JASCO ISF-531). As the samples for the absolute quantum yields measurement, the layered oxides intercalated with ethylamine were used. The layered oxides were obtained as sediments by centrifugation in the exfoliation process. The layered oxides intercalated with ethylamine obtained in the exfoliation process for $Gd_{1.4}Eu_{0.6}Ti_3O_{10}$- and $La_{0.7}Eu_{0.3}Ta_2O_7$-nanosheets are denoted as EA-intercalated $Gd_{1.4}Eu_{0.6}Ti_3O_{10}$ and EA-intercalated $La_{0.7}Eu_{0.3}Ta_2O_7$. The thickness of the exfoliated nanosheets was confirmed by atomic force microscopy (AFM, Molecular Imaging) measurements. The magnetic field in photoluminescence measurements of the nanosheet solutions was applied by using Nd−Fe−B magnets (Hitachi Metals, Ltd. NMX-44H (Br: 1.29−1.36 T)). A diagram of the photoluminescence measurement system, showing a possible orientation of the excitation source and an applied magnetic field, is illustrated in the Supporting Information S3. In all cases, the emission was detected in a direction perpendicular to the excitation source, with the magnetic field aligned along either the excitation or emission direction. Oriented films of unexfoliated powder samples of the layered perovskites were prepared by applying a homogeneous magnetic field inside the bore of an NMR spectrometer (Bruker AMX-2-500 with an Oxford magnet of 11.74 T). The oriented films were prepared as follows: The sample solution containing the sample powder (600

(26) Umemura, Y.; Shinohara, E.; Koura, A.; Nishioka, T.; Sasaki, T. *Langmuir* **2006**, *22*, 3870–3877.
(27) Nakato, T.; Miyamoto, N.; Harada, A. *Chem. Commun.* **2004**, 78–79.
(28) Nakato, T.; Miyamoto, N.; Harada, A.; Ushiki, H. *Langmuir* **2003**, *19*, 3157–3163.
(29) Miyamoto, N.; Nakato, T. *Adv. Mater.* **2002**, *14*, 1267–1270.
(30) Nakato, T.; Miyamoto, N. *J. Mater. Chem.* **2002**, *12*, 1245–1246.
(31) Gopalakrishnan, J.; Bhat, V. *Inorg. Chem.* **1987**, *26*, 4299–4301.
(32) Kudo, A.; Sakata, T. *J. Phys. Chem.* **1995**, *99*, 15963–15967.
(33) Kudo, A.; Kaneko, E. *Microporous Mesoporous Mater.* **1998**, *21*, 615–620.
(34) Kudo, A. *Chem. Mater.* **1997**, *9*, 664–669.
(35) Gopalakrishnan, J.; Bhat, V. *Mater. Res. Bull.* **1987**, *22*, 413.
(36) Machida, M.; Yabunaka, J.; Kijima, T. *Chem. Mater.* **2000**, *12*, 812–817.
(37) Toda, K.; Uematsu, K.; Sato, M. *J. Ceram. Soc. Jpn.* **1997**, *105*, 482–485.
(38) Li, C.; Murase, N. *Langmuir* **2004**, *20*, 1–4.

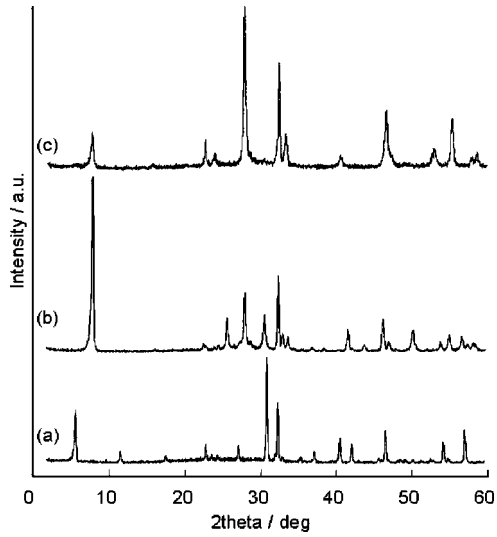

Figure 1. XRD patterns of the layered perovskite starting materials (a) $K_2Gd_{1.6}Eu_{0.4}Ti_3O_{10}$, (b) $KLa_{0.95}Eu_{0.05}Nb_2O_7$, (c) $RbLa_{0.7}Tb_{0.3}Ta_2O_7$.

mL, powder concentration 10 g/L), tetramethoxysilane (TMOS) (200 mL), and 0.1 M HCl (40 mL) were placed in a glass NMR tube (diameter: 1 cm), and then the tube was inserted into the bore of the magnet for 60 min. The sample sol solution became gelled by hydrolysis of TMOS in the magnetic field. After the reaction, the sample gel was soaked in ethanol to substitute ethanol for water in the gel and then was dried using a supercritical drier, which replaced the ethanol with CO_2. The orientation of these magnetically aligned powder samples was analyzed by using two-dimensional X-ray diffraction (2D-XRD, Bruker Smart Apex II).

Results and Discussion

The oxide starting materials, $K_2Ln_2Ti_3O_{10}$, $KLnNb_2O_7$, and $RbLnTa_2O_7$, contain single- or double-layered perovskite blocks ($[Ln_2Ti_3O_{10}]^{2+}$, $[LnNb_2O_7]^+$, and $[LnTa_2O_7]^+$) with intercalated alkali ions (K^+ and Rb^+). The A site in the perovskite blocks can accommodate various types of lanthanide ions (Ln^{3+}). Figure 1 shows XRD patterns of $K_2Gd_{1.6}Eu_{0.4}Ti_3O_{10}$, $KLa_{0.95}Eu_{0.05}Nb_2O_7$, and $RbLa_{0.7}Tb_{0.3}Ta_2O_7$ as typical starting layered oxides. The XRD peaks can be indexed to the $K_2Ln_2Ti_3O_{10}$, $KLaNb_2O_7$, and $RbLnTa_2O_7$ phases previously reported,[31,35,36] indicating that the Eu^{3+} and Tb^{3+} dopant ions substitute for A-site Ln^{3+} ions.

The intercalated K^+ or Rb^+ can be easily exchanged with protons by treatment with 1 M HCl. Exfoliation of the host layer was performed by stirring the protonated layered oxides in 0.1 M aqueous ethylamine solution. After the exfoliation reaction, the suspension was centrifuged to separate any unexfoliated particles from the suspension of exfoliated nanosheets. The supernatant (nanosheet solution) was deposited on a mica substrate by spin-coating to prepare samples for analysis by AFM. Figure 2 shows typical AFM images of isolated nanosheets ($Gd_{1.4}Eu_{0.6}Ti_3O_{10}$-, $La_{0.95}Eu_{0.05}Nb_2O_7$ -, and $La_{0.7}Tb_{0.3}Ta_2O_7$-nanosheets). The measured thicknesses of the nanosheets were 2.4 nm ($Gd_{1.4}Eu_{0.6}Ti_3O_{10}$), 1.8 nm ($La_{0.95}Eu_{0.05}Nb_2O_7$), and 1.5 nm ($La_{0.7}Tb_{0.3}Ta_2O_7$). These observed thickness are larger by 0.4−0.9 nm than those of the perovskite blocks in the host solid.[31,35,36] In general, the thickness of oxide nanosheets observed by AFM is larger than that estimated from crystallographic data because of absorption of water and amine and other systematic factors in the AFM measurements.[19,20,39–42] However, it is clear from measurements of many sheets that they represent unilamellar (rather than bi- or trilayer) particles. This indicates that the starting layered oxides are exfoliated completely by acid exchange and treatment with ethylamine.

Figure 3 shows photoluminescence spectra for the nanosheet solutions at a Eu/Ln ratio of 5/95. In this figure, the $Ln_{1.9}Eu_{0.1}Ti_3O_{10}$-, $La_{0.95}Eu_{0.05}Nb_2O_7$-, and $Ln_{0.95}Eu_{0.05}Ta_2O_7$-nanosheets are denoted as Eu5%-LnTiO, Eu5%-LaNbO, and Eu5%-LnTaO, respectively. The emission spectra were measured using an excitation wavelength of 250 nm, and the excitation spectra were obtained by monitoring the Eu^{3+} emission at 614 nm ($^5D_0-^7F_2$). The Eu5%-LnTiO (Ln: Pr, Sm, Nd, Dy) and Eu5%-GdTaO exhibited no red emission, whereas 5%Eu-LnTiO (Ln: La, Gd, Tb), Eu5%-LnNbO, and Eu5%-LaTaO exhibited red emission, as shown in Figure 3. Ozawa et al. reported the red-emitting $La_{0.90}Eu_{0.05}Nb_2O_7$-nanosheet with the same structure as that of the 5%Eu-LaNbO in Figure 3 had an excitation peak at 353 nm in the excitation spectrum.[19] However, in the case of 5%Eu-LaNbO, the intensity of the excitation at around 353 nm was very weak and a weak excitation peak appeared at around 235 nm. Especially, it should be noted that the red emission intensity of Eu-GdTiO type nanosheets is much stronger than that of the $La_{0.90}Eu_{0.05}Nb_2O_7$-nanosheet (see Supporting Information S4). Broad peaks in the region 225−330 nm in the excitation spectra in Figure 3 are assigned to energy transfer from the Ti−O network to Eu^{3+} in the nanosheet, because the excitation spectra closely resemble the band gap absorption (see Figure 6). In conclusion, the strongest red emission intensity was observed for the Eu-doped GdTiO sample. As discussed below, this emission arises from a two-step energy transfer cascade from the Ti−O network to Gd^{3+} and then to Eu^{3+}.

Figure 4 shows photoluminescence spectra of the $Gd_{2-x}Eu_xTi_3O_{10}$-nanosheet solutions at various Gd/Eu ratios (Eu-1%, Eu-5%, Eu-30%, Eu-50%, and Eu-100%). The strongest red emission intensity was observed for the Eu-30% sample. The decrease in the emission intensity for the higher Eu^{3+}-doped samples (Eu-50% and Eu-100%) is due to concentration quenching. As for the critical concentration, Toda et al. reported that the maximum emission intensity of $Na_2Ga_{2-x}Eu_xTi_3O_{10}$ by the direct excitation of Eu^{3+} ($^7F_6-^5L_6$) was experimentally obtained for $x = 0.4$, and that is also the theoretically expected optimum photoactivator concentration for this structure type by the percolation model.[43] However, the percolation model is not used in the present case, because the excitation process is based on the energy transfer from bandgap excitation to Eu^{3+}.

Green-emitting nanosheets were prepared from Tb-doped layered oxides, in the same manner as the red-emitting Eu-containing materials. All $Ln_{1.9}Tb_{0.1}Ti_3O_{10}$-nanosheets and $La_{0.95}Tb_{0.05}Nb_2O_7$-nanosheets exhibited very weak or no observable green emission, whereas the $La_{0.95}Tb_{0.05}Ta_2O_7$-nanosheets exhibited an intense green emission. In the $La_{1-x}Tb_xTa_2O_7$-nanosheets ($x = 0.01$, 0.05, 0.30, 0.50, and 1.00), the strongest

(39) Izawa, K.; Yamada, T.; Unal, U.; Ida, S.; Altuntasoglu, O.; Koinuma, M.; Matsumoto, Y. *J. Phys. Chem. B* **2006**, *110*, 4645–4650.
(40) Fukuda, K.; Nakai, I.; Ebina, Y.; Tanaka, M.; Mori, T.; Sasaki, T. *J. Phys. Chem. B* **2006**, *110*, 17070–17075.
(41) Sasaki, T.; Ebina, Y.; Kitami, Y.; Watanabe, M.; Oikawa, T. *J. Phys. Chem. B* **2001**, *105*, 6116–6121.
(42) Omomo, Y.; Sasaki, T.; Wang, L.; Watanabe, M. *J. Am. Chem. Soc.* **2003**, *125*, 3568–3575.
(43) Toda, K.; Kameo, Y.; Ohta, M.; Sato, M. J. *Alloys Compd.* **1995**, *218*, 228–232.

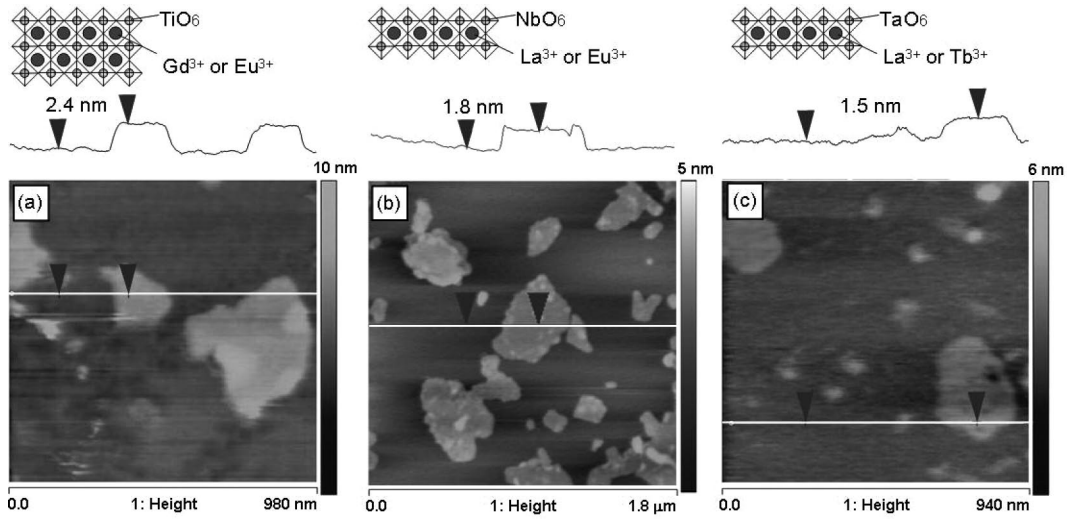

Figure 2. AFM images of the exfoliated nanosheets and proposed crystallographic orientation: (a) $Gd_{1.4}Eu_{0.6}Ti_3O_{10}$-nanosheet, (b) $La_{0.95}Eu_{0.05}Nb_2O_7$-nanosheet, (c) $La_{0.7}Tb_{0.3}Ta_2O_7$-nanosheet.

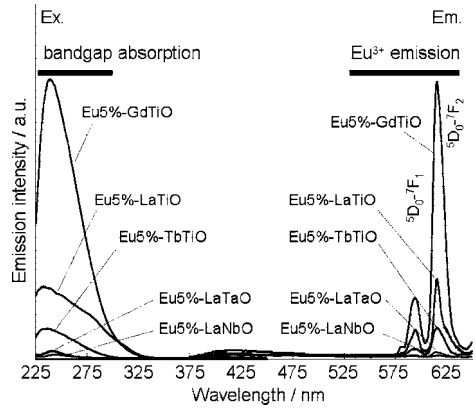

Figure 3. Photoluminescence spectra of nanosheet solutions. $Ln_{1.9}Eu_{0.1}Ti_3O_{10}$-, $La_{0.95}Eu_{0.05}Nb_2O_7$-, and $Ln_{0.95}Eu_{0.05}Ta_2O_7$- nanosheets are denoted as Eu5%-LnTiO, Eu5%-LaNbO, and Eu5%-LnTaO. λ_{ex}: 250 nm, λ_{em}: 614 nm. Concentration of the nanosheets in the solution: 2.0×10^{-5} M (formula unit).

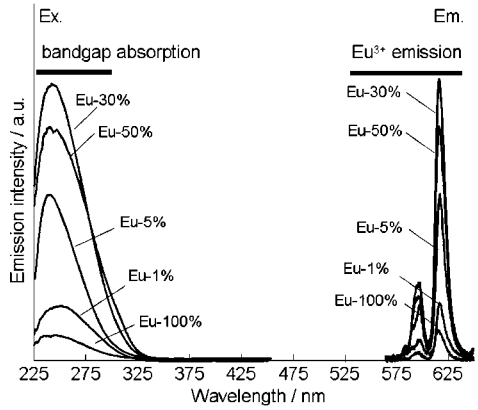

Figure 4. Photoluminescence spectra of $Gd_{2-x}Eu_xTi_3O_{10}$-nanosheet solutions at various Gd/Eu ratios (99/1: Eu-1%, 95/5: Eu-5%, 70/30: Eu-30%, 50/50: Eu-50% and 0/100: Eu-100%). λ_{ex}: 250 nm, λ_{em}: 614 nm. Concentration of the nanosheets in the solution: 2.0×10^{-5} M (formula unit).

green emission was observed for the sample with $x = 0.30$. Thus, intense red and green emissions were discovered for the $Gd_{1.4}Eu_{0.6}Ti_3O_{10}$- and $La_{0.7}Tb_{0.3}Ta_2O_7$-nanosheet solutions, respectively, in the present work.

Figure 5A and B show photoluminescence spectra for the starting material ($K_2Gd_{1.4}Eu_{0.6}Ti_3O_{10}$), the protonated form ($H_2Gd_{1.4}Eu_{0.6}Ti_3O_{10}$), and a nanosheet solution ($Gd_{1.4}Eu_{0.6}Ti_3O_{10}$-nanosheet) in the $K_2Gd_{1.4}Eu_{0.6}Ti_3O_{10}$ system. Specific red emissions of Eu^{3+} ($^5D_0-^7F_n$ ($n = 1,2$)) were observed for all the samples. Under UV irradiation, the nanosheet solution exhibited intense red emission, as shown in the photograph in Figure 5B. The emission at 592 nm is due to the magnetic dipole transition $^5D_0-^7F_1$, which is insensitive to the site symmetry. The emission at 614 nm is due to the electric dipole transition of $^5D_0-^7F_2$, induced by the lack of inversion symmetry at the Eu^{3+} site, and is much stronger than that of the transition at the $^7F_1$ site.[44–49] If the Eu^{3+} site has no inversion symmetry, the electric dipole emission is strong, and the magnetic dipole transition becomes relatively weak. On the other hand, if the Eu^{3+} site has inversion symmetry, the electric dipole emission is weak, and the magnetic dipole transition becomes relatively stronger. Thus, the ratio $I_{614nm}(^5D_0-^7F_2)/I_{592nm}(^5D_0-^7F_1)$ is affected by the site symmetry of Eu^{3+}. The ratio for the $Gd_{1.4}Eu_{0.6}Ti_3O_{10}$-nanosheet (4.5) is larger than those of $K_2Gd_{1.4}Eu_{0.6}Ti_3O_{10}$ (2.4) and $H_2Gd_{1.4}Eu_{0.6}Ti_3O_{10}$ (2.0), suggesting that the site symmetry of the Eu^{3+} site decreased. The symmetry of the Eu^{3+} site in the nanosheet can be affected by the local adsorption of chemical species and/or by physical deformation of the sheet away from planarity, both of which can occur much more easily in a unilamellar sheet than in the parent solids.

In the excitation spectra, $K_2Gd_{1.4}Eu_{0.6}Ti_3O_{10}$ and $H_2Gd_{1.4}Eu_{0.6}Ti_3O_{10}$ had several intense peaks in the 350−420 nm region as shown in Figure 5A. These peaks are assigned to intra-4f transitions of Eu^{3+} itself. The absorptions based on the intra-4f transitions of Eu^{3+} were also observed in their UV−vis absorption spectra, as shown in Figure 6A. The broad excitation peaks in the region 220−350 nm for all the samples are coincident with their band gap absorptions shown in Figure 6A, indicating that the energy transfer occurs from the Ti−O network to Eu^{3+} in the host layer in the emission process. In the case of the nanosheet, the broad excitation peak attributed to this energy transfer was blue-shifted relative to the

(44) Dejneka, M.; Snitzer, E.; Riman, R. E. *J. Non-Cryst. Solids* **1996**, *202*, 23–34.
(45) Dejneka, M.; Snitzer, E.; Riman, R. E. *J. Lumin.* **1995**, *65*, 227–245.

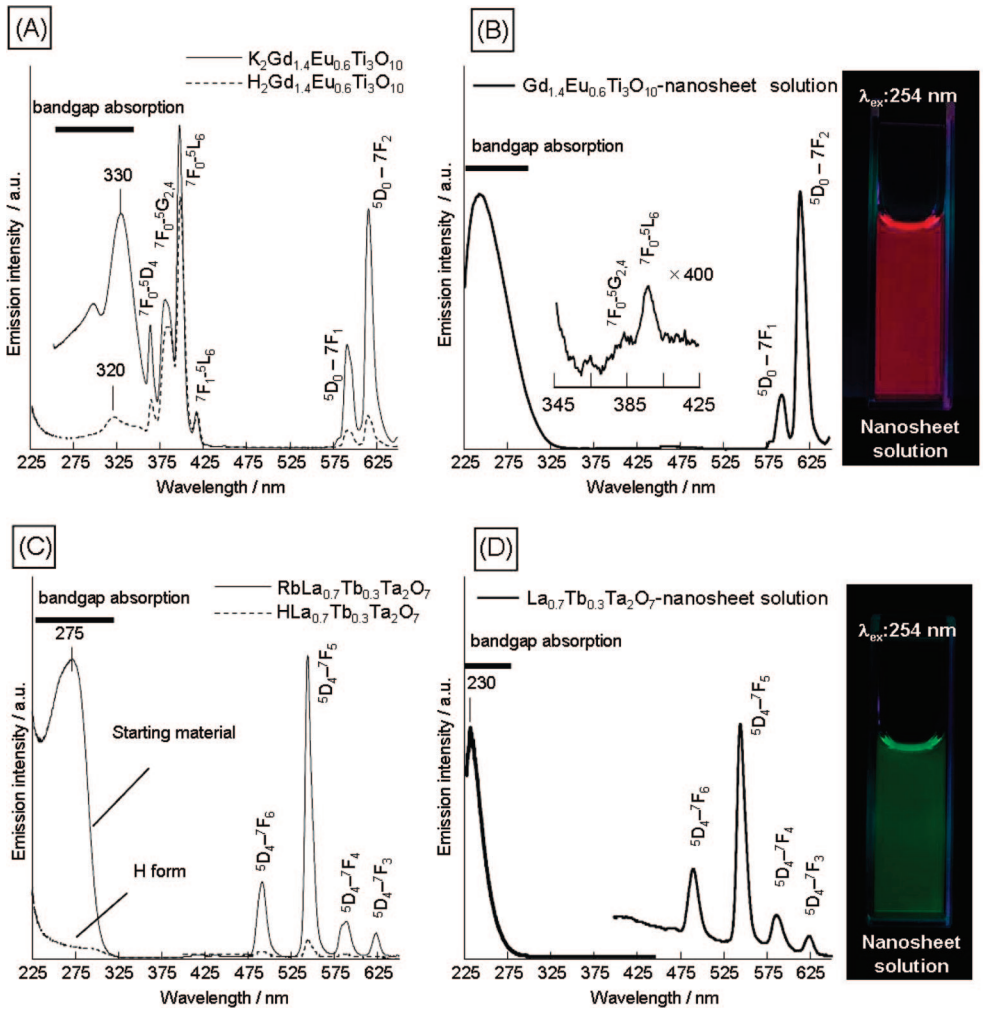

Figure 5. Photoluminescence spectra of the starting materials, their proton-exchanged forms, and nanosheet solutions in the $K_2Gd_{1.4}Eu_{0.6}Ti_3O_{10}$ and $RbLa_{0.7}Tb_{0.3}Ta_2O_7$ systems: (A) $K_2Gd_{1.4}Eu_{0.6}Ti_3O_{10}$ (λ_{ex}: 330 nm, λ_{em}: 614 nm) and $H_2Gd_{1.4}Eu_{0.6}Ti_3O_{10}$ (λ_{ex}: 320 nm, λ_{em}: 614 nm); (B) $Gd_{1.4}Eu_{0.6}Ti_3O_{10}$-nanosheet solution ($\lambda_{ex}$: 250 nm, λ_{em}: 614 nm); (C) $RbLa_{0.7}Tb_{0.3}Ta_2O_7$ (λ_{ex}: 275 nm, λ_{em}: 545 nm) and $HLa_{0.7}Tb_{0.3}Ta_2O_7$ (λ_{ex}: 275 nm, λ_{em}: 545 nm); (D) $La_{0.7}Tb_{0.3}Ta_2O_7$-nanosheet solution (λ_{ex}: 230 nm, λ_{em}: 545 nm). Concentration of the nanosheets in the solution: 2.0×10^{-5} M (formula unit). The inset photographs show red and green luminescence of $Gd_{1.4}Eu_{0.6}Ti_3O_{10}$- and $La_{0.7}Tb_{0.3}Ta_2O_7$-nanosheet solution illuminated by a UV lamp (λ: 254 nm).

$K_2Gd_{1.4}Eu_{0.6}Ti_3O_{10}$ and $H_2Gd_{1.4}Eu_{0.6}Ti_3O_{10}$ samples. This is attributed to a quantum size effect in the nanosheets. The excitation bands were red-shifted with increasing concentration of nanosheet solution (see Supporting Information S5). Thus, the main broad excitation peaks are attributed to the excitation of the band gap of the host nanosheet. It should be noted that the emission intensity derived from host excitation (at 245 nm) is ~600−1000 times stronger than that of direct Eu^{3+} excitation (at 395 nm). The chemical composition of the $Gd_{1.4}Eu_{0.6}Ti_3O_{10}$-nanosheet (from ICP analysis) was Gd/Eu/Ti = 1.27:0.61:3.0, which is close to that of the starting material ($K_2Gd_{1.4}Eu_{0.6}Ti_3O_{10}$). The relative photoluminescence efficiency of the red emission (λ_{ex}: 245 nm, λ_{em}: 614 nm) of the $Gd_{1.4}Eu_{0.6}Ti_3O_{10}$-nanosheet solution was 3.3%, and the absolute quantum yield of EA-intercalated $Gd_{1.6}Eu_{0.6}Ti_3O_{10}$ (solid sample) was 2.7% (λ_{ex}:310 nm).

Figure 5C and D show photoluminescence spectra for the starting material ($RbLa_{0.7}Tb_{0.3}Ta_2O_7$), the proton-exchanged material ($HLa_{0.7}Tb_{0.3}Ta_2O_7$), and the nanosheet solution ($La_{0.7}Tb_{0.3}Ta_2O_7$-nanosheet) in the $RbLa_{0.7}Tb_{0.3}Ta_2O_7$ system. Under UV irradiation, the nanosheet solution exhibited intense green emission, as shown in the photograph in Figure 5D. The emission peaks at 492, 545, 587, and 624 nm are assigned to $^5D_4-^7F_{j(3-6)}$ transitions of Tb^{3+}, respectively. In the excitation spectra, broad peaks were observed in the 220−350 nm region for all the samples. These peaks coincide with their band gap absorptions, as shown in Figure 6B, indicating that energy transfer occurs from the Ta−O network to Tb^{3+} in the host layer or the nanosheet. Blue shifts in the excitation peak (Figure 5D) and the UV−vis absorption (Figure 6B) of the $La_{0.7}Tb_{0.3}Ta_2O_7$-nanosheet sample are again attributed to a quantum size effect. The energy transfer is also confirmed by comparing the excitation spectra of $La_{0.7}Tb_{0.3}Ta_2O_7$- and $La_{0.7}Eu_{0.3}Ta_2O_7$-nanosheets (see Supporting Information S6). Main excitation peaks of both nanosheets were the same because of the same energy transfer from the Ta−O network. The chemical composition of the $La_{0.7}Tb_{0.3}Ta_2O_7$-nanosheet (from ICP analysis) was La/Tb/Ta = 0.31:0.09:2.0, which represents some loss of Ln^{3+} ions from the starting material ($RbLa_{0.7}Tb_{0.3}Ta_2O_7$). In the proton exchange process, some A site ions (La and Tb) are likely to be exchanged by protons. The relative photoluminescence efficiency of the green emission (λ_{ex}: 230 nm, λ_{em}: 545 nm) of the $La_{0.7}Tb_{0.3}Ta_2O_7$-nanosheet solution was about 0.9%, and the absolute quantum yield of EA-intercalated $La_{0.7}Eu_{0.3}Ta_2O_7$ (solid sample) was 2.1% (λ_{ex}:240 nm).

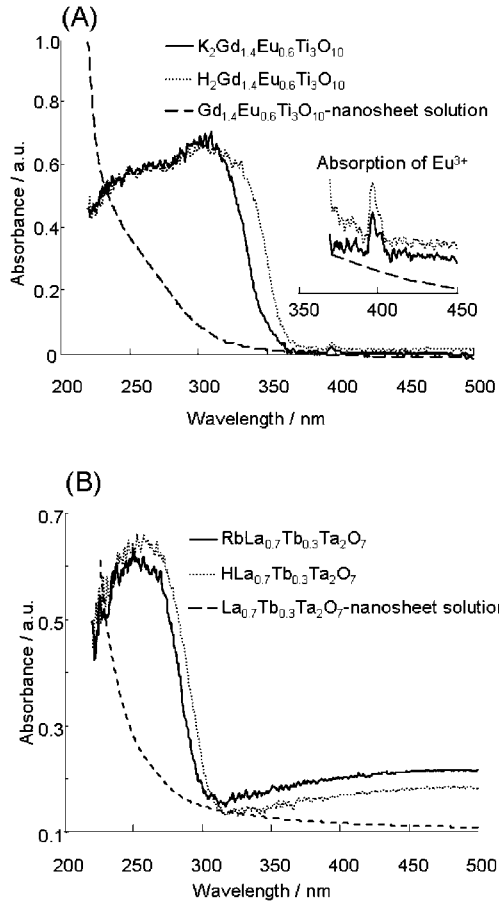

Figure 6. UV−vis absorption spectra of the starting materials, their proton-exchanged forms, and nanosheet solutions: (A) $K_2Gd_{1.4}Eu_{0.6}Ti_3O_{10}$ system, (B) $RbLa_{0.7}Tb_{0.3}Ta_2O_7$ system.

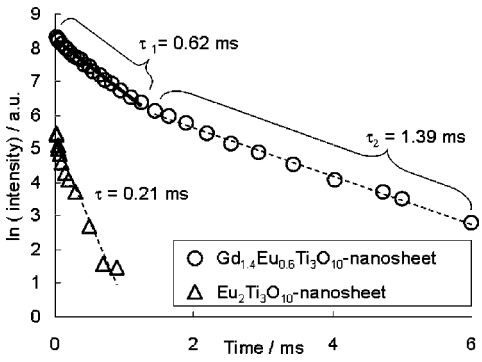

Figure 7. Time-resolved emission of the $Gd_{1.4}Eu_{0.6}Ti_3O_{10}$- and $Eu_2Ti_3O_{10}$-nanosheet solutions (λ_{ex}: 250 nm and λ_{em}: 614 nm).

Figure 7 shows emission decay curves of the $Gd_{1.4}Eu_{0.6}Ti_3O_{10}$- and $Eu_2Ti_3O_{10}$- nanosheet solutions. The $Gd_{1.4}Eu_{0.6}Ti_3O_{10}$-nanosheet containing both Eu^{3+} and Gd^{3+} in the A site had two types of decay processes with short and long luminescence lifetimes ($\tau_{Eu:1}$: 0.62 and $\tau_{Eu:2}$: 1.39 ms). On the other hand, the $Eu_2Ti_3O_{10}$-nanosheet containing only Eu^{3+} in the A site had only one decay process with a short luminescence lifetime (τ: 0.21 ms). On the basis of these results, a model for the energy transfer in the $Gd_{1.4}Eu_{0.6}Ti_3O_{10}$-nanosheet can be developed as illustrated in Figure 8. The high luminescence efficiency of the $Gd_{2-x}Eu_xTi_3O_{10}$-nanosheet is based on the efficient energy transfer via Gd^{3+}, because the presence of Gd^{3+} promotes the emission of Eu^{3+} as noted above. Energy transfer from Gd^{3+}

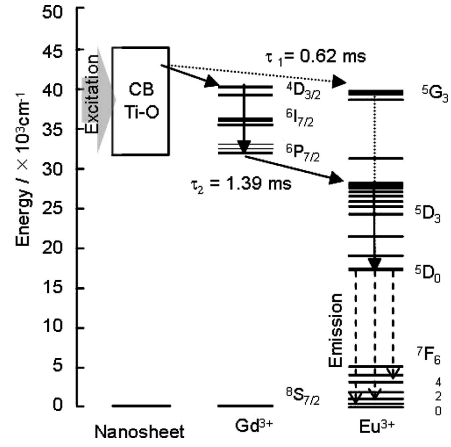

Figure 8. A model for the energy transfer leading to photoluminescence in the $Gd_{1.4}Eu_{0.6}Ti_3O_{10}$-nanosheet system.

to Eu^{3+} has been previously reported for other materials.[50–54] The energy of the Ti−O band gap excitation in the nanosheet will be transferred to the ^4D_j, ^6I_j, and ^6P_j levels of Gd^{3+} (first step) and then transferred to Eu^{3+} (second step). Thus, the energy transfer via Gd^{3+} from the Ti−O network to Eu^{3+} results in strong red emission of Eu^{3+}. The short lifetime component of the $Gd_{1.4}Eu_{0.6}Ti_3O_{10}$- and $Eu_2Ti_3O_{10}$-nanosheet emission, which is common to both materials, can be assigned to direct energy transfer from the Ti−O network to Eu^{3+} in the nanosheet. Consequently, the long luminescence lifetime is assigned to the two-step energy transfer from the Ti−O network to Gd^{3+} and then to Eu^{3+} in the nanosheet.

The layered perovskite starting materials for the $Gd_{1.4}Eu_{0.6}Ti_3O_{10}$- and $La_{0.7}Tb_{0.3}Ta_2O_7$-nanosheet suspensions are strongly attracted to the side of their container in the inhomogenous field of a hand-held Nd−Fe−B magnet, because of the paramagnetism of the Gd^{3+} and Tb^{3+} ions. The theoretical magnetic moments of Gd^{3+} and Tb^{3+} are 7.94 and 9.72 μ_B, respectively. Because of the strong paramagnetism of these materials, we studied their orientation in a strong homogeneous magnetic field. In this case, the reorientation of the paramagnetic particles is a result of the anisotropy of their magnetic susceptibility. The orientation of the particles induced by the magnetic field was fixed using a sol−gel technique that we have developed for diamagnetic lamellar solids.[55] Figure 9 shows 2D-XRD patterns of $K_2Gd_{1.4}Eu_{0.6}Ti_3O_{10}$ aligned in a strong magnetic field (∼11.7 T), with the orientation fixed by gelling the suspension with tetramethylorthosilicate (TMOS). In 2D-XRD, the diffraction pattern is obtained in two dimensions of reciprocal space simultaneously. For oriented samples, diffraction rings coalesce

(46) Lu, Z.; Wang, J.; Tang, Y.; Li, Y. *J. Solid State Chem.* **2004**, *177*, 3075–3079.
(47) Rainho, J. P.; Carlos, L. D.; Rocha, J. *J. Lumin.* **2000**, *87−89*, 1083–1086.
(48) Kropp, J. L.; Windsor, M. W. J. *Chem. Phys.* **1965**, *42*, 1599–1609.
(49) Ananias, D.; Ferreira, A.; Rocha, J.; Ferreira, P.; Rainho, J. P.; Morais, C.; Carlos, L. D. *J. Am. Chem. Soc.* **2001**, *123*, 5735–5742.
(50) Yokosawa, N.; Nakazawa, E. *Jpn. J. Appl. Phys., Part 1* **2003**, *42*, 7373–7375.
(51) Lu, C.-H.; Huang, C.-H. *Chem. Lett.* **2004**, *33*, 1568–1569.
(52) Liu, Y.; Ye, C.; Qian, G.; Qiu, J.; Wang, M. *J. Lumin.* **2006**, *118*, 158–164.
(53) Zhang, X.; Zhang, J.; Liang, L.; Su, Q. *Mater. Res. Bull.* **2005**, *40*, 281–288.
(54) Pang, M. L.; Lin, J.; Fu, J.; Cheng, Z. Y. *Mater. Res. Bull.* **2004**, *39*, 1607–1614.
(55) Eguchi, M.; Angelone, M. S.; Yennawar, H.; Mallouk, T. E., in preparation.

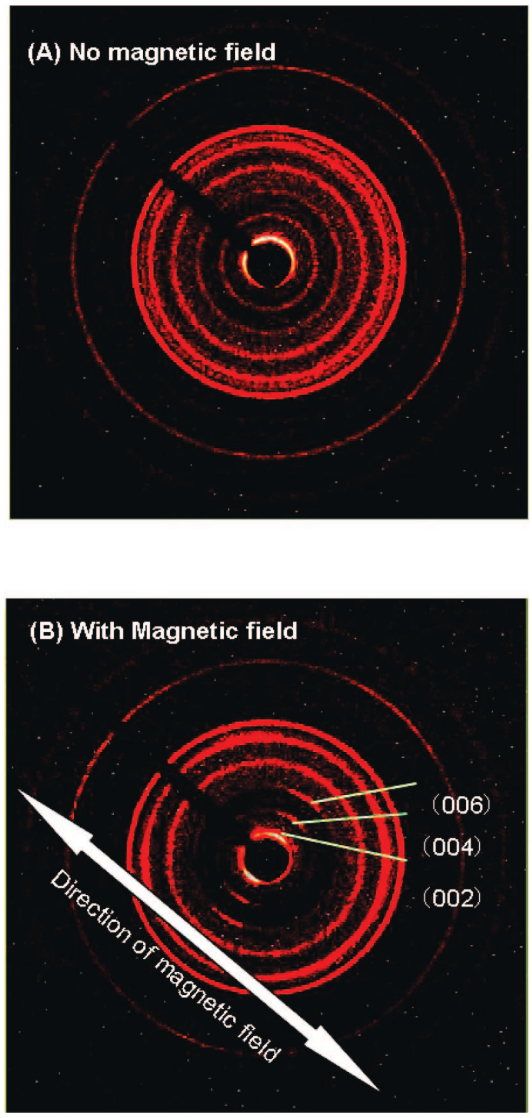

Figure 9. 2D-XRD patterns of $K_2Gd_{1.4}Eu_{0.6}Ti_3O_{10}$ suspensions gelled by TMOS hydrolysis under a strong homogeneous magnetic field (11.7 T): (A) no magnetic field, (B) with magnetic field.

into narrow arcs, and the intensity pattern can be analyzed to reveal the orientation of anisotropic particles.[56,57] The direction of the applied magnetic field is indicated by the arrow (Figure 9B). In the absence of an applied magnetic field, the sample showed ring-like diffraction patterns (Figure 9A), whereas several narrow diffraction peaks were observed under the applied magnetic field in a direction perpendicular to the applied magnetic field (Figure 9B). These narrow peaks were indexed to (00n) reflections, meaning that the *c*-axis of $K_2Gd_{1.4}Eu_{0.6}Ti_3O_{10}$ is perpendicular to the direction of the magnetic field. This behavior is similar to our observations with the diamagnetic layered solid $K_4Nb_6O_{17}$, which also orients with the layer stacking axis perpendicular to the magnetic field. The magnetic alignment of diamagnetic sheets derived from $K_4Nb_6O_{17}$ is due to its weak diamagnetic anisotropy. Diamagnetic anisotropy is considered by Uyeda to originate from the spatial distribution of bonding electrons in the solid. Calculations of this effect for

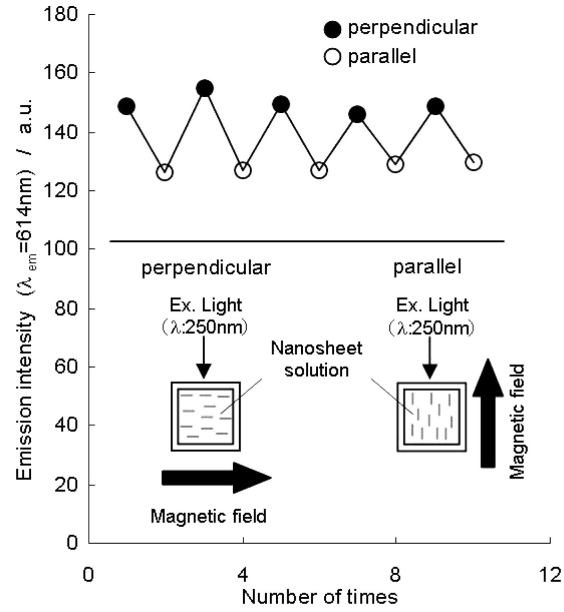

Figure 10. Red emission intensity modulation of $Gd_{1.4}Eu_{0.6}Ti_3O_{10}$-nanosheet solutions with perpendicular or parallel magnetic field applied (λ_{ex}: 250 nm and λ_{em}: 614 nm).

tetrahedrally and octahedrally bonded oxide crystals are consistent with experimental observations of their preferred orientation in strong magnetic fields.[58] The observed alignment of the parent solids, which indicates that they possess anisotropy in their magnetic susceptibility, suggests that the $Gd_{1.4}Eu_{0.6}Ti_3O_{10}$- and $La_{0.7}Tb_{0.3}Ta_2O_7$-nanosheets might also be aligned in magnetic fields.

Figure 10 shows the change in the red emission intensity (614 nm) of the $Gd_{1.4}Eu_{0.6}Ti_3O_{10}$-nanosheet solution under magnetic fields applied parallel and perpendicular to the excitation direction. The red emission intensity increased in the perpendicular magnetic field and decreased when the excitation and magnetic field were collinear. Based on the 2-D XRD data obtained for the parent solids, we hypothesize that the sheets are preferentially oriented with the layer plane away from the magnetic field direction. This orientation is shown schematically in Figure 10 for the idealized case of perfectly oriented sheets; in reality some thermally induced randomization of the orientation will occur. With regard to the magnetic alignment of nanosheets, it has been reported that superparamagnetic colloidal plates synthesized from $Ca_2Nb_3O_{10}$-nanosheets and Fe_3O_4 nanoparticles have a magnetic anisotropy with the easy axis in the plane of the plates and the hard axis perpendicular to it.[59] The plates are rotated around an in-plane axis by rotating the external magnetic field around an axis parallel to the plate and are rotated around an out-of-plane axis by rotating the magnetic field around an axis perpendicular to the plate. By analogy, in our system similar changes in the orientation of nanosheets should occur as the magnetic field is reoriented. The magnetically induced change in alignment of the nanosheets presumably brings about a change in absorption or in scattering of absorbed and/or emitted light. The green emission of the $La_{0.7}Tb_{0.3}Ta_2O_7$-nanosheet solution could also be moduled under a magnetic field (see Supporting Information S7). Thus, the intensities of both the red- and green-emitting nanosheets can be modulated by

(56) He, B. B.; Preckwinkel, U.; Smith, K. L. *Adv. X-Ray Anal.* **2000**, *43*, 273–280.
(57) Melosh, N. A.; Davidson, P.; Chmelka, B. F. *J. Am. Chem. Soc.* **2000**, *122*, 823–829.
(58) Uyeda, C. *Phys. Chem. Miner.* **1993**, *20*, 77–81.
(59) Kim, J. Y.; Osterloh, F. E.; Hiramatsu, H.; Dumas, R. K.; Liu, K. *J. Phys. Chem. B* **2005**, *109*, 11151–11157.

applying a ~1 T magnetic field. This effect may be due to alignment or switching of the nanosheet emission in optical devices.

Conclusions

Luminescent perovskite nanosheets were prepared by exfoliation of layered oxides: $K_2Ln_2Ti_3O_{10}$, $KLnNb_2O_7$, and $RbLnTa_2O_7$ (Ln: lanthanide ion). $Gd_{1.4}Eu_{0.6}Ti_3O_{10}$- and $La_{0.7}Tb_{0.3}Ta_2O_7$-nanosheets exhibited an intense red and green emission, respectively, under UV illumination at an energy greater than that of the corresponding host oxide band gap. Both emissions arise from energy transfer within the nanosheet. The red emission intensity of the $Gd_{1.4}Eu_{0.6}Ti_3O_{10}$-nanosheet was much stronger than that of $La_{0.90}Eu_{0.05}Nb_2O_7$-nanosheets reported previously.[19] The high emission intensity is based on a two-step energy transfer cascade from the Ti−O network to Gd^{3+} and then to Eu^{3+}. This is the first report of such an energy transfer cascade in nanosheet. The green emission is based on the direct energy transfer from the Ta−O network to Tb^{3+} in the $La_{0.7}Tb_{0.3}Ta_2O_7$-nanosheet. To the best our knowledge, this is also the first report of green emission in an oxide nanosheet. With the addition of intense red and green emissions it is now possible to achieve all emission colors, because nanosheets with an intense blue emission have been developed previously.[18] Although the mechanism is not yet understood in detail, we find that both red and green emission intensities could be modulated by an applied magnetic field, which changes the orientation of the nanosheets in solution.

Acknowledgment. This work was supported by a Grant-in-Aid for Scientific Research (No. 440, Panoscopic Assembling and High Ordered Functions for Rare Earth Materials, and No. 16080215) from the Ministry of Education, Culture, Sports, Science and Technology, and by the National Science Foundation under Grant CHE-0616450.

Supporting Information Available: S1: structural model of the starting materials. S2: sample preparation for ICP analysis. S3: photoluminescence measurement system under magnetic field. S4: comparison of red emission intensities between different types of nanosheets. S5 and S6: assignment of energy transfer for nanosheets. S7: green emission intensity modulation of $La_{0.7}Tb_{0.3}Ta_2O_7$-nanosheet solutions in a magnetic field. S8: reagent purity. This material is available free of charge via the Internet at http://pubs.acs.org.

JA7114772